

Pol Reddy Kukutla and B.V.S.S.S Prasad*

Numerical Study on the Secondary Air Performance of the Film Holes for the Combined Impingement and Film Cooled First Stage of High Pressure Gas Turbine Nozzle Guide Vane

<https://doi.org/10.1515/tjj-2017-0022>

Received June 28, 2017; accepted July 12, 2017

Abstract: The present numerical investigation of Leading Edge (LE) Nozzle Guide Vane (NGV) is considered with five rows of impingement holes combined with five rows of film cooled for the secondary coolant flow path analysis. The coolant mass flow rate variations in all the LE rows of the film holes externally subjected to the hot main stream were obtained by making a three-dimensional computational analysis of NGV with a staggered array of film cooled rows. The experiments were carried out for the same NGV using Particle Image Velocimetry technique to determine the effused coolant jet exit velocity at the stagnation row of film holes as mentioned in reference [Kukutla PR, Prasad BVSSS. Secondary flow visualization on stagnation row of a combined impingement and film cooled high pressure gas turbine nozzle guide vane using PIV technique, J Visualization, 2017; DOI: 10.1007/s12650-017-0434-6]. In this paper, results are presented for three different mass flow rates ranges from 0.0037 kg/s to 0.0075 kg/s supplied at the Front Impingement Tube (FIT) plenum. And the mainstream velocity 6 m/s was maintained for all the three coolant mass flow rates. The secondary coolant flow distribution was performed from SH1 to SH5 row of film holes. Each row of a showerhead film hole exit coolant mass flow rate varied in proportion to the amount of coolant mass rates supplied at the FIT cooling channel. The corresponding minimum and maximum values and their film hole locations were altered. The same behaviour was continued for the coolant pressure drop and temperature rise from SH1 to SH5 row of film holes. Owing to the interaction between hot main stream and the coolant that effuses out of the film holes, occasional presence of hot gas ingestion was noticed for certain flow

rates. This caused nonlinear distribution in mass flow, pressure drop and temperature rise. The minimum flow rate results estimate oxidation of NGV material near the film cooled hole. And the effect of hot gas ingestion on the ejected film cooled jet which would recommends effective oxidation resistant material which in turn leads to better durability of the NGV surface.

Keywords: nozzle guide vane, CFD, secondary air analysis, jet impingement cooling, film cooling

PACS® (2010). (47.27.nf: Flows in pipes and nozzles)

Introduction

The Nozzle Guide Vanes (NGVs) of a modern gas turbine engine are cooled in order to keep their surface temperature in the allowable limits. The compressor air bleed which is used to cool the vane should be used in such a way that it gives maximum heat transfer rates with minimum pressure drop. The combined impingement and film cooling technique is widely used in a cooled high pressure first stage NGV in order to enhance the heat transfer and for improving the durability of the NGV surface material. Where the jetting action is made on the rear side of a nozzle guide vane by means of orifice jet impingement flows and then finally effused out from the external surface of the film holes, which makes a boundary layer over the vane surface to protect the mainstream effect.

Although sufficient Conjugate Heat Transfer (CHT) and aerodynamics studies of a cooled gas turbine NGV have been reported, most investigate the effect of secondary coolant flow mechanism, the multi-physics flow field coupled with interaction of jets and mainstream flow which necessitates the investigation for the aero thermal design cooling system.

A combination of impingement and film cooling approach with conjugate heat transfer obtained through computational fluid dynamics is applied in order to improve the performance of jet impingement and film cooling holes for the performance of a gas turbine high pressure NGV, coupled with the 3D viscous solver for the gas flow field. For

*Corresponding author: B.V.S.S.S Prasad, Turbomachines Laboratory, Department of Mechanical Engineering, Indian Institute of Technology Madras, Chennai, Tamil Nadu, 600036, India, E-mail: prasad@iitm.ac.in

Pol Reddy Kukutla, Turbomachines Laboratory, Department of Mechanical Engineering, Indian Institute of Technology Madras, Chennai, Tamil Nadu, 600036, India, E-mail: polireddyk01@gmail.com

a high pressure gas turbine nozzle guide vane, it is used to rapidly predict and evaluate the aerodynamic and heat transfer performances of the film cooled jets.

According to the computation results, there will be alternative ways definitely proposed for the improvement of design, which includes the variation of the more appropriate coolant flow mass rate entering at the front impingement insert.

Goldstein et al. [1] observed that in case of 7-jet and 3-jet arrays the outer jets moved outward due to cross-flow, hence maximum Nusselt number occurs away from the jet center. For these arrays, higher Nusselt number occurs with the smaller spacing than with larger spacing. In case of multiple (seven) jets with low H/D values, flow interaction among jets causes the mixing induced turbulence to penetrate toward the center of individual jets; resulting in the absence of local minima at the stagnation point.

Honami et al. [2] presented detailed measurements of the laterally injected jet on the velocity/temperature field by a hot-wire anemometer and a thermo-resistance meter and the surface temperature field by the temperature-sensitive liquid crystal. The tests were conducted at three mass flux ratios, 0.5, 0.85, and 1.2. The laterally injected jet has an asymmetric structure with a large scale of vortex motion on one side caused by the interaction with the primary stream, but suppressed on the other side. And also there was a little contribution to the film cooling on one side with the vortex motion, whereas high film-cooling effectiveness was obtained on the other side. Asymmetry was promoted with mass flux ratio increased, resulting in low film-cooling effectiveness.

Huang et al. [3] presented detailed heat transfer distributions for an array of in-line jets impinging orthogonally on a target plate with three exit cross flow orientations. The measurements are carried for each exit orientation, at four Reynolds numbers which range from 4.8×10^3 to 1.83×10^4 . A transient liquid crystal technique was used to measure the detailed heat transfer coefficients on the target surface. Results show that the heat transfer coefficient distributions are significantly affected by cross flow direction. A cross flow direction where the flow exits both sides of the chamber provides the highest Nusselt numbers on the surface. Jet impingement is least affected by the oncoming cross flow compared to the other two cases.

The effect of exit flow orientation on heat transfer to a target surface with film holes for multiple jet impingement arrays has been investigated. The results are compared with the target surface without film holes by cross flow direction are presented by Ekkad et al. [4] and also in [5]. presented effects of impinging jet angle on target surface heat transfer distributions for an array of

impinging jets. The detailed distributions clearly indicate the jet angle and cross flow exit direction effects. Although local differences in Nusselt numbers are significantly affected by jet inclination, the inclined jets produce more uniform Nusselt number distributions than the orthogonal jets, which may be considered a positive result for some practical applications.

A three-dimensional computational study was performed by Heidmann et al. [6] for a realistic film cooled turbine vane. The simulation includes the flow regions inside the coolant plena and film cooling holes apart from the mainstream flow. The detailed information from the film hole flows was reported in the form of hole exit profiles. The peak mass flux is influenced by both external static pressure variations and the hole orientation. The round holes exhibit the peak tends that were skewed both toward the downstream direction and toward the injection angle of the hole. The suction side holes exhibit the greatest skewing because these two effects are in the same direction. But the shaped holes exhibit a complex behavior with an intense local maximum in mass flux near the leading edge of the hole. The center of the hole contributes very little mass flux, as compared to the sides and trailing edge supply coolant that has followed the hole wall around from the leading edge. The shaped holes are effective in producing a low-velocity, uniform film layer. All holes exhibit a relatively flat stagnation temperature profile except for the centers of the shaped holes, where a negligible mass flux allows greater influence of the hotter free stream. The round holes have exit profiles of momentum, and stagnation temperatures were generalized, allowing external vane computations to the model mainstream flow. The complex flow in the shaped holes makes it difficult to generalize their exit properties for input to an external vane calculation, but a high span-wise uniform flow was produced, especially in a staggered arrangement, when modeled by a two-dimensional wall function or modified slot flow with downstream inviscid wall condition.

Gritsch et al. [7] observed a profound effect of coolant cross-flow Mach number for a perpendicular coolant supply direction on film-cooling effectiveness. For a cylindrical hole with low blowing ratio, the lateral spreading was increased while the effectiveness was decreased in the centerline portion when compared with the stagnation (base) plenum case. Similar improved performance was observed at high blowing ratios compared to the base plenum case. However, for shaped holes with internal cross-flow, the jet entering the diffuser section of the hole was highly disturbed, causing poor performance of the diffuser and leading to a less uniform cooling film.

Gao et al. [8] performed experiments with detailed heat transfer coefficient distributions that are presented for the jet to jet impingement arrays in the stream wise as well as spanwise spacing of four and eight-hole diameters then later linearly stretched jet-impingement arrays. Heat-transfer coefficients are typically higher for the varying holes on most of the test plate as expected, except for the first two rows where uniform holes produce higher heat-transfer coefficients as a result of increased jet flow.

Katti and Prabhu [9] experimentally investigated the effect of local heat transfer distribution on the target plate due to confined impingement of an in-line rectangular array of multiple jets with spent air flow exiting in two opposite directions. Spent flow from upstream jets imposes a cross-flow on the downstream jets.

Oh et al. [10] carried out combined impingement and film cooling study on a full coverage film cooled flat plate. They compared the cooling effectiveness with normal and inclined film holes. They carried out a parametric study by varying the jet Reynolds number and the jet-to-plate spacing. They found the effectiveness to increase with blowing ratio and film holes with inclination showing superior performance. An experimental investigation was conducted on the cooling effectiveness of full-coverage film cooled wall with impingement jets. Film cooling plate was made of stainless steel, thus the adiabatic film cooling effectiveness and the cooling effect of impingement jet underneath the film cooling plate were comprised in the cooling effectiveness. Infra-red camera was used to measure the temperature of film cooled surfaces. Experiments were conducted with different film cooling hole angles, such as 35° and 90° . Diameters of both film cooling holes and impinging jet holes were 5 mm. The jet Reynolds number base on the hole diameter (Re_d) ranged from 3,000 to 5,000 and equivalent blowing ratios (M) varied from 0.3 to 0.5, respectively. The distance between the injection plate and the film cooling plate was 1, 3 and 5 times of the hole diameter. The stream-wise and span-wise hole spacing to the hole diameter ratio (p/d) were 3 for both the film cooling hole plate and the impingement jet hole plate. The 35° angled film cooling hole arrangement showed higher film cooling effectiveness than the 90° film cooling hole arrangement. As the blowing ratio increased, the cooling effectiveness was enhanced for both the 35° almost constant regardless of H/d , whereas $H/d=1$ showed a minimum value for the angled film cooling hole.

The PIV measurements were coupled with detailed film cooling effectiveness distributions on the flat plate

obtained using a steady state, Pressure Sensitive Paint (PSP) technique by Wright et al. [11]. The PIV measurements showed the increased mixing of the coolant jet with the mainstream at the elevated free stream turbulence level resulting in a reduction in the jet to effectively protect the film cooled surface.

Jessen et al. [12] experimentally investigated for a zero and an adverse pressure gradient configuration using the PIV technique for the turbulent flow field of a multi-row film cooling configuration. The geometric parameters such as pitch and hole shape were kept constant. Two different mass flux ratios, $MR=0.28$, and $MR=0.48$ were considered for the detailed comparison of the mean flow field and the turbulence statistics, which show a very good agreement between the measurements and the simulations.

El-Gabry et al. [13] presented the measurements of velocity and turbulence fluctuations and stresses in a large-scale film cooling model at two nominal blowing ratios of 2 and 1 using Hotwire anemometry. Results were obtained for blowing ratios of up to 2 in order to capture severe conditions in which the jet was lifted and the velocity vectors and contour at the stream-wise planes exhibited the distinct kidney vortex renders reduced effectiveness of the film cooling as the vortex pair pushes the hot gas from the mainstream down toward the wall. The jet deflection was more at the lower blowing ratio of 1, but the film was not in completely attached position. Velocity fluctuations in the mainstream direction were significant at high blowing ratio up to 30% of the mainstream velocity and about half that intensity for the low blowing. The fluctuations in the hole-to-hole direction were smaller at about 10% intensity for the high blowing ratio case and about half that for the lower blowing ratio. The wall-normal direction was found the significant velocity fluctuations and locally in some of the regions exceed 25% of the mainstream velocity.

Panda and Prasad [14] investigated the effect of solid thermal conductivity on conjugate heat transfer from a flat plate with combined impingement and film cooling both experimentally and computationally. A flow configuration with multiple staggered rows of cylindrical film holes and a matrix of impingement holes were considered. A thermo chromic liquid crystal technique was used in the experiment to measure the surface temperature of the plate. Results from the conjugate heat transfer study are presented for three blade materials: A, B, and C with thermal conductivities of 0.2, 1.5, and 15W/mK respectively with three blowing ratios of 0.6, 1.0, and 1.6. And the corresponding mainstream Reynolds number was varied from 49,050 to 130,800; and the coolant jet Reynolds

number was kept constant at 825. The computations for the impingement surface reveal multiple peaks and valleys in the heat flux and temperature plots. Material C experienced significant changes in the values of impingement surface heat flux and temperature with blowing ratio, whereas these changes were only minor for material A. On the interaction surface, convective heat flux values were the lowest for material A and progressively increased with increasing thermal conductivity. However, the effectiveness values varied significantly for material A in the stream-wise direction. A good agreement was found between the effectiveness distributions obtained from the measurements and the computations.

Experimental and computational studies were carried out by the Pujari et al. [15] in two-dimensional five-vane cascade having four passages. Each vane had a chord length of 228 mm and the pitch distance between the vanes was 200 mm. The vane internal surface was cooled by dry air supplied through both the FIT and AIT impingement inserts: the mass flow through the impingement chamber was varied, for a fixed spacing (H) to jet diameter (d) ratio of 1.2. The surface temperature distributions, at certain locations of the vane interior, were measured by pasting strips of liquid crystal sheets. The internal temperature distribution and the internal heat transfer characteristic for an NGV were determined with multiple impingements jets and film cooling. The results indicate that with the increase in coolant mass flow, the internal surface temperature decreases; however, the surface temperature reduction is non-uniform and also depends on external film cooling effectiveness. For the increased mainstream flow Reynolds number causes an increase in the internal surface temperature when the coolant mass flow is kept constant.

Chandran and Prasad [16] carried out a computational and experimental study on the leading edge region of a combined impingement and showerhead film cooled gas turbine nozzle guide vane. The local effectiveness values obtained by the computations agreed well with the experimental data from IR thermography. The effect of blowing ratio on the overall effectiveness was found to be strongly dependent on the vane material conductivity. And also the effect of blowing ratio was different toward the pressure and suction sides of the stagnation region. However, the overall effectiveness was found to decrease by about 12% and 6% for low and high conducting materials, respectively, with an increase in mainstream Reynolds number from $Re = 4.8 \times 10^5$ to 14.4×10^5 .

Experimental and numerical investigations were presented by Singh et al. [17] for the average Nusselt number augmentation with cooling of a circular cylinder

maintained at a constant heat flux by a circular air jet impingement with a semi-circular concave confinement at the bottom of the heated cylinder. The parametric investigations were reported for the four different values of the nozzle to cylinder distance of the flow confinement for different values of jet Reynolds number. The results reveal that the up to 24% increase in local Nusselt number as compared to the confinement without an opening was observed at the rear stagnation point due to the presence of the semi-circular concave confinement for $h/d=16$ and the smallest radius of the confinement, which corresponded to the smallest spacing between the cylinder and the confinement. And the average Nusselt number increased by about 17% at $h/d=16$, for all the Reynolds numbers and h/d values with smallest confinement radius, due to the confinement.

Singh et al. [18] investigated both the experimental and numerical studies on jet impingement cooling of circular cylinder with circular, square and rectangular nozzles to understand the effects of the nozzle shape on fluid flow and heat transfer characteristics. In this study, a fixed hydraulic diameter was selected for all the three nozzle shapes. Reynolds number based on the hydraulic diameter, was kept constant for constant mass flow rate irrespective of the nozzle shape. Parametric studies were conducted with both fixed Re and fixed mass flow rate. The results reveal that for a fixed Reynolds number, the rectangular nozzle shows better Nusselt number at the stagnation point and nearby regions. However, for the case of fixed mass flow rate, the circular nozzle shows better performance compared to the other nozzle shapes. In the case of fixed Reynolds number, the mass flow rate through the rectangular nozzle was much higher compared to the other nozzle shapes. As less mass flow rate is preferred in cooling of thermal systems, it is better to compare nozzles with the fixed mass flow rate instead of fixed Reynolds number. On the other hand, if both the Re and mass flow rate were constant, local Nusselt number distributions for different nozzle shapes were significant only up to $z/D=2$ in the axial directions and up to 45° in the circumferential directions. The stagnation point Nusselt number decreased as h/Dh increased for all the nozzle shapes and Reynolds number considered due to the entrainment of the surrounding air, which reduced the jet velocity. Even though the mass flow rate increased due to air entrainment in the main jet stream, the mean velocity of the jet decreased considerably.

Pujari et al. [19] investigated both the experimental and computational studies on the interior side heat transfer of an NGV subjected to combined impingement and film cooling. The domain of the study was a two-

dimensional five-vane cascade having a space chord ratio of 0.88. The results show that, when the blowing ratio was increased by increasing the coolant flow rate, the average internal surface temperature decreased. However, when the blowing ratio was varied by increasing the mainstream Reynolds number, the internal surface temperature increased. Further, the temperature variations were different all along the internal surface from the leading edge to the trailing edge and were largely dependent on the coolant flow distributions on the internal as well as the external surfaces.

Singh et al. [20] reported both experimental and numerical studies on double circular air jet impingement cooling of a heated circular cylinder to understand flow and heat transfer characteristics. The surface of the heated cylinder was maintained at a constant heat flux condition. Various parametric studies were done for the range of Reynolds number from 10,000 to 25,000. The Reynolds number was considered based on the nozzle diameter. The ratio of the diameter of the nozzle to the diameter of the heated cylinder (d/D) was maintained at 0.208. The effect of non-dimensional distance between double the jets (s/d) was investigated for the range of 4 to 20 and the ratio of the non-dimensional distance between the nozzle exit and the circular cylinder surface (h/d) was investigated for the range of 4 to 16. The results reveal that there was no appreciable change noticed in the stagnation point Nusselt number with a change in s/d . However, with an increase in s/d , the average Nusselt number over the cylinder surface was also found to increase. In this study, the effect of flow confinement below the heated cylinder on heat transfer was also investigated. Both experimental and numerical studies show that confinement at the bottom of the cylinder increases heat transfer.

Kukutla and Prasad [21] have recently reported an analysis of the local jet velocity distribution for a combined impingement and film cooled high pressure first stage nozzle guide vane, using flow visualization and PIV assisted measurement. The measurements including flow visualization were performed on the stagnation row of an NGV to understand the complex flow pattern. The PIV technique was used to measure the effused coolant jet exit velocity field in two-dimensional vertical planes. The computations were performed by ANSYS FLUENT14.5 SOLVER using SST $k-\omega$ turbulence model. Three laboratory test cases that correspond to inlet coolant mass flow rates of 0.0032, 0.0045 and 0.0054 kg/s, at the region of a FIT, were studied. The numerical results for the span-wise coolant velocity at stagnation row of the film holes agreed well with the PIV

experimental data on the same vane configuration. These results indicate that the distribution of local film cooling jet flow rate is not uniform across the nine film cooling jets of a stagnation row for the given FIT plenum coolant mass flow rate. It mainly depends on the uniform cross-section of the FIT plenum in the span-wise direction and the quantity of coolant supplied at the FIT plenum. Near the stagnation region, the atmospheric air momentum is very small, so the effused coolant jets from stagnation (SH3) row subjected to the higher jet deflection at the baseline condition. While at the higher FIT plenum coolant flow rates, the air momentum slightly increases, subjected to the coolant jet is deflected. This non-linear variation of the jet's velocity distribution was observed at the stagnation row showerhead holes for all the three plenum conditions. It is because of the contraction or expansion of the potential core length of the jet in the span-wise direction.

It is evident from the above available literature, that hitherto there were no experimental or computational investigations performed in the secondary coolant flow paths analysis at each SH row of the film holes for the combined impingement and film cooled high pressure first stage nozzle guide vane. However, a few of the studies were done on curvature and as well as flat plate. The usage of these available results for the actual showerhead designs of the high pressure first stage NGV makes it very difficult. Moreover, the film cooling jet on the LE of the vane external surface has the advantage that the mainstream flow field may be symmetric with respect to the stagnation point. Furthermore, the film holes ejected jet velocities depend on the coolant flow, mainstream flow turbulent intensities and as well as mainstream velocity conditions. Therefore, the present paper focuses on the detailed secondary flow pressure loss and temperature rise at each SH row of the film holes for three different coolant mass flow rates for an FIT plenum configuration.

The broad objective of this paper is to study the effect of three different coolant mass rates supplied at the FIT plenum and the mainstream velocity on (i) span-wise coolant mass flow rate distribution (ii) span-wise coolant pressure drop distribution and (iii) distribution of the span-wise coolant static temperature rise. These results estimate oxidation of NGV material near the film hole and the effect of hot gas ingestion prompting to provide effective oxidation resistant material which in turn causes better durability of the NGV surface at each row of the film holes on the leading edge of the typical cooled NGV surface; these are reported in this paper

Nozzle guide vane geometry details CFD methodology

The NGV for the present study was developed from the geometric details of the high pressure first stage gas turbine nozzle guide vane. The geometry had several two-dimensional planes and sectional details. It comprised two impingement inserts: FIT and Aft Impingement Tube (AIT). The total surface of the NGV was divided into three parts: the leading edge surface, the pressure surface and the suction surface with thirteen film cooling rows on the vane surface. The FIT and AIT were developed by extruding the mid-section profiles by 100 mm. The FIT and AIT had 217 and 144 number of impingement holes respectively, distributed along their surfaces as indicated in Figure 1(b). The thickness of FIT was 0.4 mm and that of AIT was 0.7 mm. The gap between the impingement inserts and the rear side of the vane was 2.8 mm throughout.

Hence there were a total of 156 number of film holes distributed throughout the NGV surface and 361 number of impingement holes provided on the impingement inserts. The distribution of all these holes can be better understood from the isometric view of the NGV and inserts as shown in Figure 1 (a). The NGV was designed in such a way that the coolant enters the FIT and AIT inlets, passes through the impingement holes and hits the rear side of the NGV as small jets. After impingement, the coolant from the FIT effuses out of the five rows of leading edge shower head holes (SH5, SH4, SH3, SH2 and SH1), two rows of suction side film holes (SS1 and SS2) and through two rows of pressure side film holes (PS3 and PS4). The coolant that enters the AIT, after impingent, effuses out through the remaining film holes on the suction side (SS3 and SS4) and pressure side (PS1 and PS2).

Computational domain

The computational domain consists of three zones:

Fluid Zone 1: Coolant flow to the film holes through impingement holes,

Solid Zone 2: Solid regions of the NGV that correspond to the thickness of the vane and impingement tube inserts.

Fluid Zone 3: Mainstream flow includes interacting flow with film cooling around the NGV.

The cooled gas turbine guide vane geometry model was imported from Solidworks to Gambit. The void spaces inside NGV and those inside the film and impingement holes were converted into fluid volumes. An extension of 100 mm was provided on either side of the realistic NGV so as to avoid the side wall effects. Hence net width of the domain was 300 mm. the spacing between the vanes was maintained to get the same S/Ch ratio of 0.88. The domain was extended to 1.5 chord length upstream and downstream of the NGV in order to avoid specifying inlet and exit flow conditions close to the region of study. All the edges and faces of the geometry model were made suitable for very fine grid generation.

The computational domain shown in Figure 2 replicates the cascade model adopted for the experiments. All the geometric specifications of the nozzle guide vane were used for the computational studies on the secondary coolant flow analysis of the showerhead rows of the film holes of an NGV. The stagnation row of all the film cooled holes effused coolant jet velocities, considering atmospheric pressure on the vane surface, were measured using PIV technique at Internal Combustion Engines

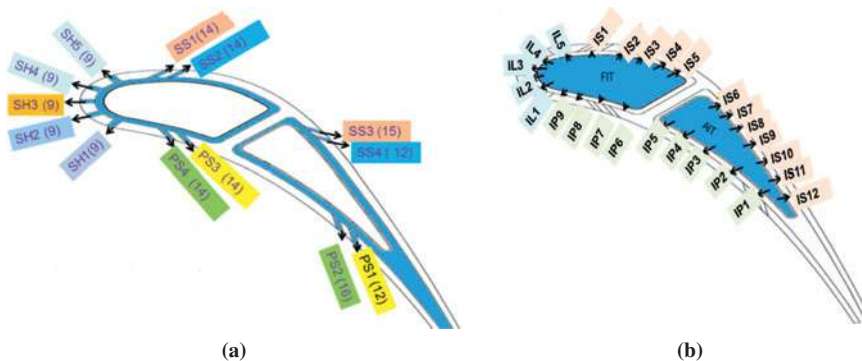


Figure 1: Nozzle Guide Vane Details. (a) NGV outer surface with film holes marked. (b) FIT and AIT with impingement holes marked.

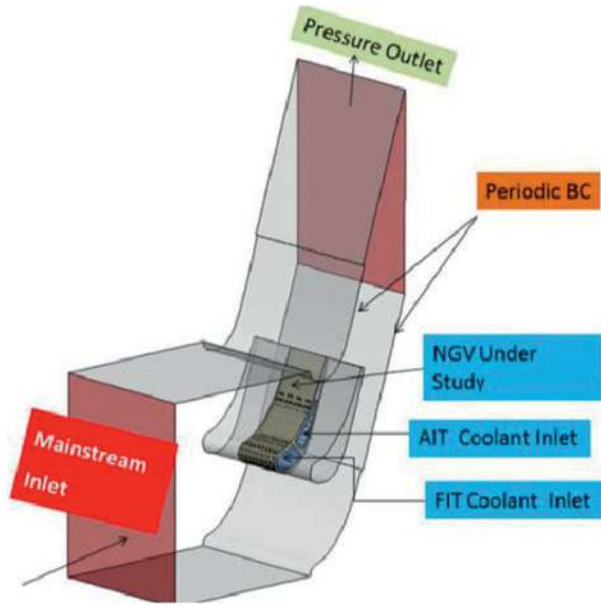


Figure 2: Computational domain.

Laboratory, Dept. of Mechanical Engineering in the Indian Institute of Technology Madras. The same was computationally validated by the Kukutla and Prasad [21]. In addition to this, various parametric studies were performed on the effect of the mainstream velocity, temperature and mainstream turbulent intensity of the stagnation row film cooled holes for the ejected jet velocities.

Meshing

The mesh for computational study, as shown in Figure 3, was generated using commercial software Gambit 2.4.6. A hybrid mesh was generated in the fluid zones and the solid zone mentioned in the previous section. For flow past turbine airfoils, direct resolution of the near wall flow was preferred instead of using wall functions to predict the boundary layer profiles. The near wall turbulence models require a low y^+ value that should be less than 2, with a refined mesh close to the vane surface. Hence, a three-dimensional boundary layer type mesh, as can be seen from Figure 3, was provided on the vane surface where the interaction between the mainstream and the coolant was to be captured with high accuracy.

Grid independence study

The Grid sensitivity study was carried out with three mesh sizes: coarse, medium and fine as given in Table. 1. The

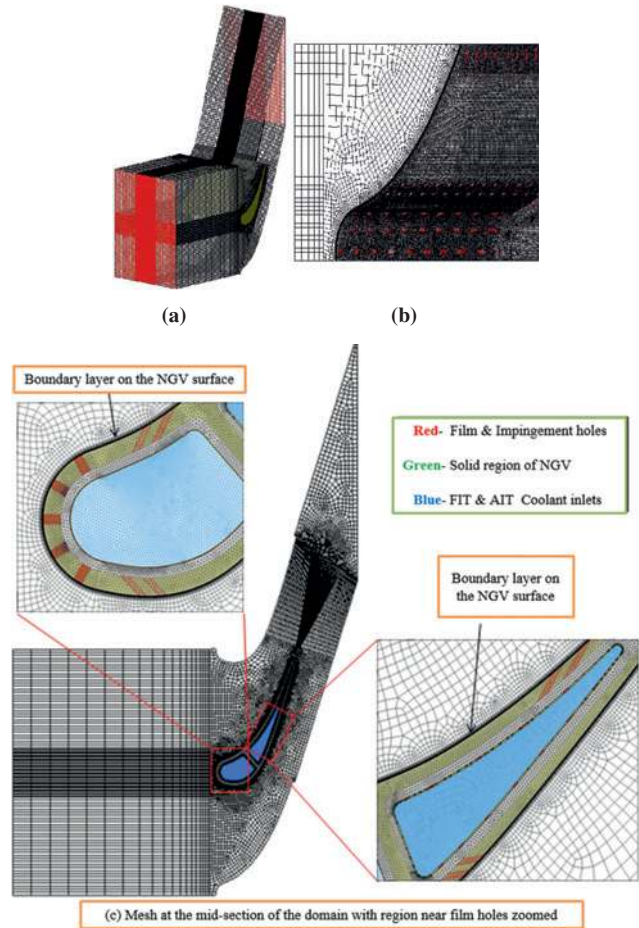


Figure 3: Mesh used for computation. (a) Mesh given at the full domain (b) Mesh in the region close to the NGV surface.

Table 1: Details of cells used for meshing.

	No. of cells (Millions)	Value of y^+
Fine	15.1	0.5
Medium	12.7	0.8
Coarse	9.8	1.5

coarse mesh had approximately 9.8 million cells and the wall y^+ was close to 1.5. The medium and fine meshes had cells close to 12.7 million and 15.1 million respectively and their wall y^+ values were improved to 0.8 and 0.5 respectively by further refining the near wall mesh. The span-wise averaged effectiveness at various stream-wise locations of the vane was calculated and plotted in Figure 4. When the mesh was improved from coarse to medium, a maximum difference in the effectiveness value of about 3% was witnessed. However, a further refinement of mesh showed a maximum difference of less than 1%

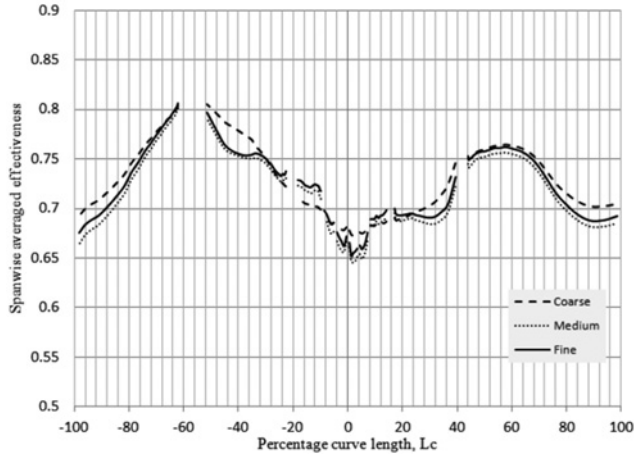


Figure 4: Grid Independence study.

between medium and fine mesh effectiveness values. For an additional 2.4 million cells, this difference was negligibly small. Hence, the medium mesh was found optimum and adopted for the present computational model. In this mesh, a y^+ value less than 0.8 was ensured throughout the vane surface and at the film holes exit by providing a three-dimensional boundary layer with the first row height of 0.02 mm and a growth factor of 1.2 for 20 rows.

Governing equations

The fundamental governing equations used for simulation are the continuity, momentum (Navier-Stokes) and energy equations along with the equations for modelling the turbulence quantities.

The three dimensional conjugate heat transfer problem is formulated as follows

Continuity equation: The conservation equation of mass is:

$$\nabla \cdot (\rho \vec{v}) = 0$$

Momentum equation: Conservation of momentum in an inertial (non-accelerating) reference frame is

$$\nabla \cdot (\rho \vec{v} \vec{v}) = -\nabla p + \nabla \cdot (\bar{\tau}) + \rho \vec{g}$$

Where p is the static pressure and $\rho \vec{g}$ is the gravitational body forces respectively.

Shear Stress tensor, $\bar{\tau} = \mu \left[\left(\nabla \vec{v} + \nabla \vec{v}^T \right) - \frac{2}{3} \nabla \cdot \vec{v} \right]$
Energy equation:

$$\nabla \cdot (\vec{v}(\rho E + p)) = \nabla \cdot \left(k_{eff} \nabla T - \sum_j h_j \vec{J}_j + (\bar{\tau}_{eff} \cdot \vec{v}) \right)$$

$$\text{Where } E = h - \left(\frac{p}{\rho} \right) + \left(\frac{v^2}{2} \right)$$

Solution methodology

The conservation equations that are necessary to be solved for simulation of the three-dimensional conjugate heat transfer problem are those of mass, momentum and energy. These equations are selected from Fluent 14.5 code, consistent with the assumptions of steady, incompressible, constant thermophysical property fluid with negligible viscous dissipation, radiation and natural convection. The κ - ω Shear Stress Transport (SST) model is adopted for turbulence modelling. Panda and Prasad [12] initially reported combined impingement and film cooled studies on a flat plate. According to their study, κ - ω SST model predicted the flow interactions very well and showed good correspondence with their experimental results. κ - ω SST model also has the advantage that it automatically switches between κ - ω model and κ - ϵ model for predicting the flow characteristics close to the wall and away from the wall respectively. In the current model, as the value of y^+ is brought down below unity, the full advantage of low-Reynolds number formulation is taken and the boundary layer is directly resolved, thereby avoiding the limitations of wall functions.

Boundary Conditions:

The following Boundary conditions specified for the present study are,

- i) Velocity inlet condition at the mainstream inlet
- ii) Pressure outlet condition at mainstream outlet
- iii) Mass flow inlet condition at FIT and AIT coolant inlets
- iv) No slip boundary condition at the wall
- v) Periodic boundary condition at the internal walls
- vi) Conjugate thermal condition at the walls of the NGV and
- vii) Adiabatic boundary condition at the symmetry planes.

$$I = 0.16 (\text{Re}_{Dh})^{(-1/8)}$$

where Re_{Dh} is the Reynolds number calculated based on the hydraulic diameter of the FIT duct.

The thermal condition at the NGV walls is specified differently as follows:

- (a) Conjugate boundary condition at the solid plate,

$$k_{Solid} \frac{\partial T_{Solid}}{\partial y} = k_{Fluid} \frac{\partial T_{Fluid}}{\partial y}$$

$$T_{solid} = T_{fluid},$$

- (b) Adiabatic condition where the solid portion of the NGV (represented in green color in Figure 3 is removed and the following condition is specified on the NGV internal and external surfaces:

$$\frac{\partial T_{Solid}}{\partial y} = 0$$

Simulation

In order to solve the governing equations with appropriate boundary conditions, the commercial finite volume based commercial ANSYS FLUENT 14 code along with mesh generation code Gambit 2.4.6 is chosen. The overall simulation procedure has the following steps. SIMPLE algorithm is used for pressure velocity coupling. The Standard interpolation scheme is used for pressure. The Second order upwind scheme is applied for momentum and energy and first-order upwind scheme is used for turbulent kinetic energy and specific dissipation rate. The solution is considered to be converged when the maximum residual value is in the order of 10^{-4} for continuity, and 10^{-6} for the momentum, turbulence quantities and for the energy equation. Further, the area weighted average temperature of the interaction surface is continuously monitored, so that the variation remains within 0.1% for 1000 consecutive iterations. All the computations are continued till the cooled plate temperature has attained steady state.

Results and discussion

The results obtained are in the span-wise direction of each film cooled row of an NGV. The mainstream velocity is maintained at 6 m/s for the below-mentioned test cases. The three different FIT plenum coolant mass flow rates are as follows: Test condition 1 (C1): 0.0037 kg/s, Test condition 2 (C2): 0.005 kg/s and Test condition 3 (C3): 0.0075 kg/s.

Leading edge rows coolant mass flow rate distributions

The percentage mass flow rates distribution for the leading edge showerhead film holes in the SH5 row for the three coolant flow rates supplied by the FIT plenum are as shown in Figure 5. As the coolant flow passes from hub to tip in the span-wise direction it can be noticed that the minimum flow rate happens at the first hole of the SH5 row for all the three FIT plenum coolant supply conditions. This is because the jet exit is retarded as the potential core length of the jet is subjected to expansion in the span-wise direction. This makes the ring vortex which is formed within the hole move away from the jet centreline. Therefore, the first hole experiences minimum m_j/m_c for a given plenum flow rate.

The percentage flow rate is suddenly reduced at the seventh hole for both the 0.0037 kg/s and 0.005 kg/s

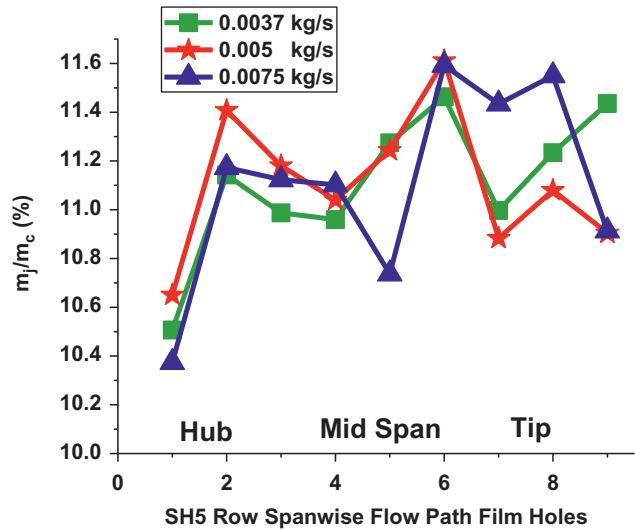


Figure 5: Span wise coolant flow rate variation at SH5 row holes.

respectively. Similarly, the same behaviour is observed at the fifth hole in the case of 0.0075 kg/s. The maximum percentage mass flow rate is arrived at the sixth hole for all the coolant mass flow rates supplied at the front impingement tube passage. This is because of the strong counter-rotating vortice formation associated with the jetting effect that weakens at the higher FIT plenum coolant mass flow rates. The same is explained by Heidmann [6] and Chandran [16].

Figure 6 shows the span-wise coolant mass flow rate ratio variation in the SH4 row showerhead film holes, which is positioned with S/C ratio of 0.099, toward the suction surface of the NGV. The lowest coolant mass flow ratio is observed at the first hole within the range of 8.16% to 8.25%. This is because the first hole of the cooling jet is under expansion so that the minimum coolant flow rate exists under the three different coolant supply conditions. The highest coolant jet mass flow rate ratio is noticed at the eighth hole. This happens because the jet is accelerated as the potential core of the jet is contracted in the span-wise direction. This necessitates the ring vortex to move toward the jet centerline, which in turn causes to increase the jet mass flow rate. The positions of the lowest and highest coolant mass flow rates are not altered for the other two higher plenum coolant flow rates. At all the three different plenum flow rates, the eighth film hole is noticed with the highest mass flow ratio ranging from 12.09% to 11.77% in the span-wise direction. The m_j/m_c ratio gradually decreases from the baseline condition to the highest FIT plenum flow rate. As we can see from Figure 6, the fourth and fifth holes exhibit approximately the same mass flow

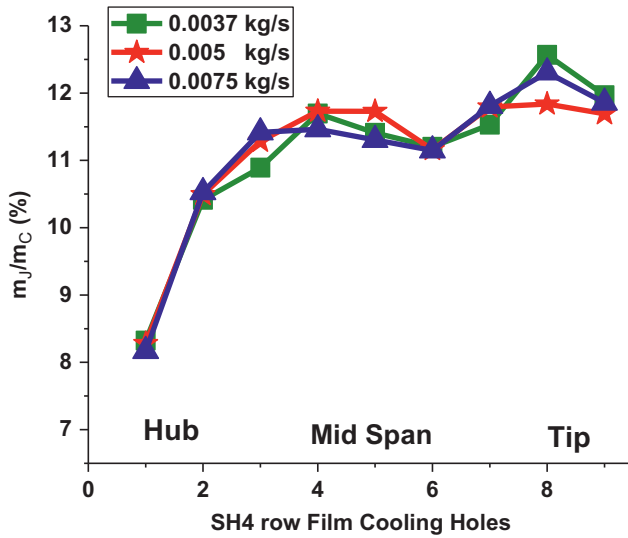


Figure 6: Span wise coolant flow rate variation at SH4 row holes.

rate at the higher plenum flow rate conditions. The reason for this is, the jets have neither acceleration nor retardation at these film hole positions, as the jet exit has a higher turbulence intensity of the shear layer

The span-wise coolant jet mass flow rate variation for the stagnation (SH3) row film holes at the leading edge region of the vane external surface is as shown in Figure 7. All the three different FIT coolant mass flow rates were noticed with meager amounts of coolant flow rate at the first hole, as the jets always try to contact with NGV surface. The minimum m_j/m_c ratio variation ranges from 9.62% at the baseline condition to 10.47% at the high FIT plenum coolant flow rate of 0.0075 kg/s.

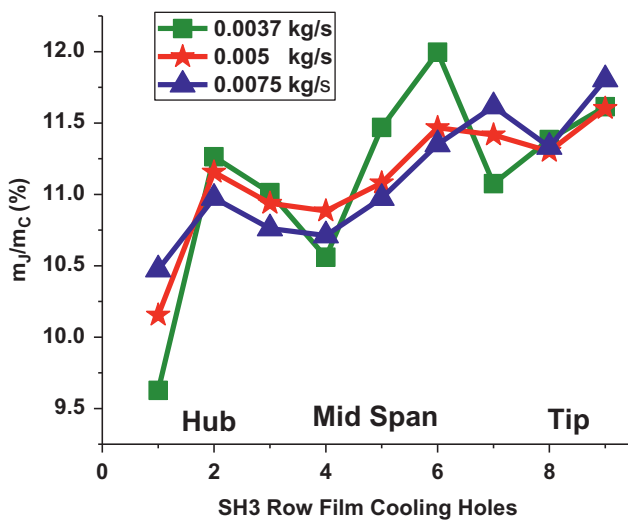


Figure 7: Span wise coolant flow rate variation at SH3 row holes.

Moreover, there is a sudden decrease in the values that are observed at the fourth and seventh holes for the baseline condition. It is due to sudden reduction of the impinging jet cross-flow momentum that causes an abrupt change in the film cooled jet structure within these holes, which primarily depends on the effect of instability of the jet flow. However, the highest m_j/m_c ratio is identified at the sixth hole with 12.00% under the base line condition. As $S/C=0$, the jet deflections attained by the cross-over phenomena of the jets are insufficient to push out the flow rates which come out from the SH3 row showerhead holes

It happens due to the initial disturbance in the jets caused by the vortices that appeared earlier. For the subsequent increase in the remaining two plenum coolant mass flow rates, the position of the maximum value is changed to the ninth hole. The maximum percentage coolant mass flow rates range from 11.60% to 11.80%. Apart from this, the third and fourth holes, positioned at the mid-span of the NGV, have almost the same m_j/m_c ratio. As these jets at these locations are not subjected to either expansion or contraction, there exists no variation in the local coolant jet mass flow rate.

Figure 8 depicts the SH2 row film cooled holes positioned at the S/C ratio 0.099 on the PS of the NGV surface. From Figure 7, it is observed that the local coolant jet mass flow rate behaviour is similar to the SH4 row (refer Figure 5). It is because both SH4 and SH2 rows are symmetrical in S/C ratio. The baseline coolant mass flow rate supplied at FIT plenum pronounced that the minimum coolant flow rate is observed at the first hole with value of 8.01% and the maximum coolant jet mass flow

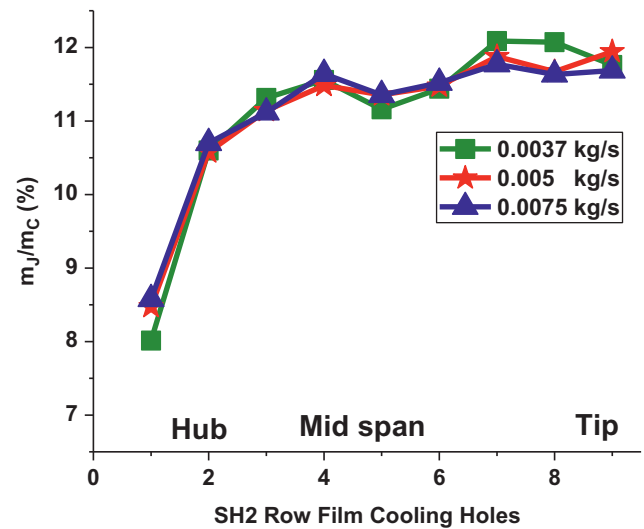


Figure 8: Span wise coolant flow rate variation at SH2 row holes.

rate is observed at the seventh hole has 12.09%, which is located at the tip region of the NGV. The minimum amount of coolant jet mass flow ratio improved, while at the same time the maximum values decrease with increased FIT plenum mass flow rates. As we have observed, even for the higher FIT plenum coolant mass flow rates, the minimum m_j/m_c ratio value occurs at the first hole position, except that these values are improved. On the contrary, the maximum coolant m_j/m_c ratio value is significantly altered for the increased plenum flow rates. The percentage of the minimum and maximum m_j/m_c magnitudes for the second case lie between 8.47% and 11.94%. At this FIT flow rate condition, the maximum flow rate exists at the ninth film hole, which is located at the tip region. Finally, for the FIT plenum flow rate of 0.0075 kg/s, the minimum and maximum m_j/m_c ratio covers between 8.58% and 11.77%. This happens at the seventh hole of the SH2 row, located at the tip region of the vane surface.

These nonlinear variations of the local coolant jet mass flow rates are consistently repeated for all the three plenum flow rates under the constant mainstream velocity. This is due to the presence of the large number of ring vortices that disturb the film cooled jet exit mass flow rate at lower plenum coolant mass flow rates. The ring vortices are rolled up and grow in size as they are convected downstream for the increased FIT flow rates.

Figure 9 shows the SH1 row span-wise coolant jet mass flow rate variation in terms of percentage. The SH1 row is positioned with the S/C ratio of 0.12 on the PS of the NGV. The behavior resembles with the SH5 row film cooled holes (refer Figure 4); the only difference is that the minimum value is slightly decreased and maximum value is moderately improved under the baseline condition. This happens because of the location of the SH1 row. Furthermore, a majority of the flow rate which comes from the showerhead holes accelerates toward the SS rows than the PS rows. The same behavior persists for the increased coolant flow rates supplied at the FIT cooling channel. The minimum coolant jet mass flow rate occurs at the first film hole, while at the same the maximum coolant jet flow rate arrives at the ninth hole for all the three different FIT plenum flow rates. Contractions and expansions of the potential core of the jet in the radial or span-wise direction are observed at the ninth and first holes for all the three FIT plenum flow rates. The spacing between the jet particles streamlines is reduced where the ring vortex formation rotates toward the jet centerline; this happens at the tip of the holes.

These results imply high metal temperature near the hub region holes that subsequently causes the oxidation

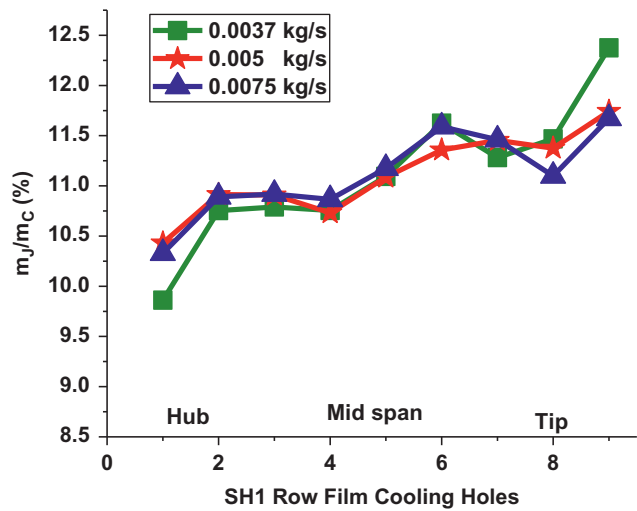


Figure 9: Span wise coolant flow rate variation at SH1 row holes.

of the material. This necessitates the stronger oxidation resistance NGV material around this region. On the other hand, higher thermal gradients near the tip region of the holes. This causes the formation of hot spots, which in turn leads to the reduction of durability of the NGV material.

The percentage distribution of coolant mass flow rate at the leading edge showerhead rows named SH1, SH2, SH3, SH4 and SH5 are shown in the Figure10. Figure 10 depicts each showerhead row total coolant mass flow rate ratio distribution in the span-wise direction. The total coolant mass flow ratio is higher at the SH5 and SH4 rows, which are positioned on the SS region, than the

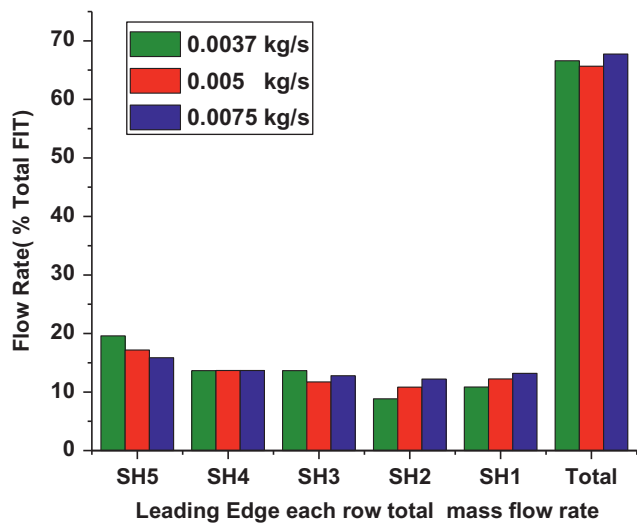


Figure 10: Span wise mass flow rate on the entire the leading edge of showerhead holes.

SH1 and SH2 rows, which are covered on the PS of the NGV. This is mainly because of the increase in jet cross flow momentum caused by the deflection of the jets toward the SS due to the favorable pressure gradient for the SH4 and SH5 rows. The inverse effect is identified for the SH1 and SH2 rows, due to the adverse pressure gradient on the PS rows of the NGV. This behavior is repeated for the next two test cases of increased FIT plenum coolant mass flow rates. Therefore, overall 65% to 67% of the total supplied FIT coolant mass flow rate effuses from all the showerhead film holes. Therefore, the increase in plenum coolant flow rate is influenced by the film coolant jetting action and the variation in the slantwise inclination. Singh et al. (18) also reported that for a constant mass flow rate, the circular nozzle shows better performance compared to the other nozzle shapes as minimum amount of mass flow rate is preferred in cooling of thermal systems. Therefore it is always better to compare nozzles or orifices with the constant mass flow rate instead of constant Reynolds number.

Leading edge rows coolant pressure drop distributions

Figure 11 shows the secondary air coolant pressure drop distributions at SH5 row film cooled holes in the spanwise direction. The static pressure drop is calculated as the difference between the static pressure at the inlet of the film hole and static pressure at the exit of the film hole. This is due to the arrangement of the five impingement jet rows (IL1 to IL5) on the convex shape of the FIT

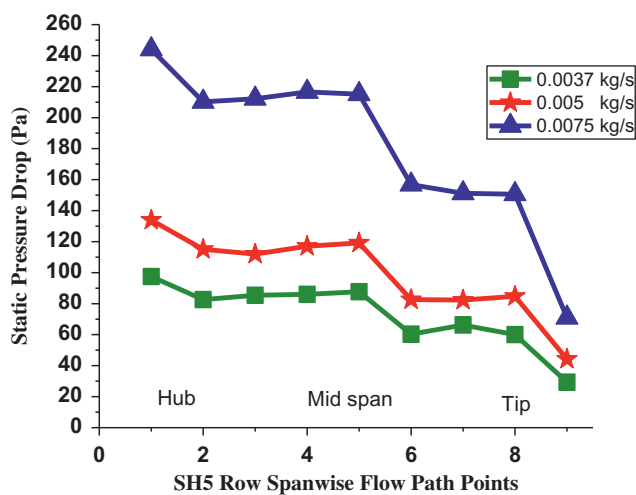


Figure 11: Span wise coolant pressure drop variation at SH5 row holes.

cooling plenum. Each IL row has fifteen holes with diameter of 2.49 mm in the span-wise direction. Hence the static pressure available is not uniform at the inlets of all the SH5 row film holes. Similarly, at the exit each film cooled jet is influenced by the mainstream velocity. It is observed that for a baseline condition (0.0037 kg/s), coolant air pressure drop variation for the SH5 row holes in the span-wise direction has minimum static pressure drop value of 29.34 Pa, which occurs at the ninth hole, located in the tip region. At the same time, the maximum static pressure drop value is 97.48 Pa, identified at the first film hole, which is located in the hub region of the NGV.

For the increased FIT plenum flow rates, minimum and maximum ΔP s values occur at the ninth and first hole of this row, except that the magnitudes of ΔP s increase due to an increase of mainstream velocity in this row. The sixth hole, at which the sudden reduction in the pressure drop is noticed for all the three plenum flow rates as the effect of multiple impinging action of the jets at the mid-span is ineffective.

When the FIT coolant flow rate is maintained as 0.005 kg/s, then the minimum and maximum static pressure drop magnitudes are increased to 44.19 Pa and 133.91 Pa. In the case of 0.0075 kg/s, the corresponding minimum and maximum static pressure drop values are obtained as 70.88 Pa and 244.06 Pa. All the SH5 row showerhead holes are predicted with positive static pressure drop values. This gives the information that there is no effect of hot gas ingestion for these holes. At higher coolant flow rates, all the SH5 row showerhead holes exhibit increased coolant static pressure drop and this necessitates the reduction of typically cooled nozzle guide vane surface temperature.

The SH5 film holes indicate that the minimum and maximum coolant static pressure drop magnitudes are higher for all the plenum conditions. It depends on the convex shape of the LE curvature at the SH5 row. This is because of the increase in S/C ratio and the effect of a higher mainstream velocity at this location.

Figure 12 shows the SH4 row film cooled holes static pressure drop variation. The baseline coolant mass flow rate supplied at the LE circuit of the cooling channel, along the flow path points of the SH4 row with minimum ΔP s of 19.59 Pa, occurred at the first hole, located at the NGV hub region. And the maximum ΔP s of 51.02 Pa is predicted at the second film hole from the NGV hub. The quantitative information of the minima and maxima ΔP s change for the higher FIT plenum coolant mass flow rates, but interestingly these locations or positions of the film holes are not altered for all the three plenum

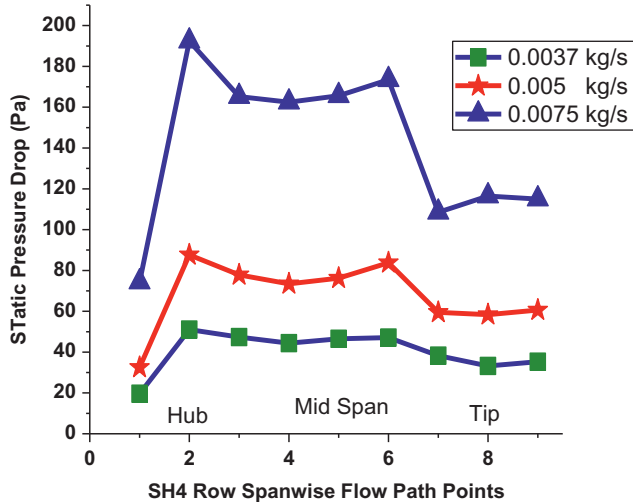


Figure 12: Span wise coolant pressure drop variation at SH4 row holes.

conditions. It is due to both the inlet and exit static pressure variation for all the SH4 film holes under higher coolant mass flow rates at the plenum that lie within 9.65% to 12.32%. The minimum and maximum coolant static pressure drop values obtained for the increased plenum mass flow rate of 0.005 kg/s and 0.0075 kg/s are as follows: 32.51Pa; 87.67 and 74.33Pa; 192.34Pa respectively.

The streamwise distance of the SH4 film cooled row is very nearer to the stagnation (SH3) row. Therefore, the minimum and maximum static pressure drop values are increases proportional to the amount of secondary air supplied at the FIT plenum. This is because of the both the minimum and maximum static pressure values are at inlet of the each hole is increases and inverse behaviour is observed at the exit of the each hole. Furthermore, influence of the mainstream flow on the coolant ΔP_s variation at SH4 row showerhead holes are smaller. In addition to the, amount of coolant mass flow rate supplied at the FIT Plenum.

The coolant static pressure drop distribution at the stagnation row (SH3) showerhead holes is depicted in Figure 13. The minimum ΔP_s values are observed at the ninth hole, positioned at the tip of the row subjected to all the three FIT plenum flow rates. However, the maximum ΔP_s value is observed at the third hole under the baseline condition, and for the increased FIT flow rates, the position is shifted to the first hole of this row. The minimum coolant ΔP_s values are noticed as 12.67, 22.68 and 35.07Pa. The minimum pressure difference across the ninth film cooled jet hole at the tip is primarily due to insufficient crossflow momentum of the jets for all the

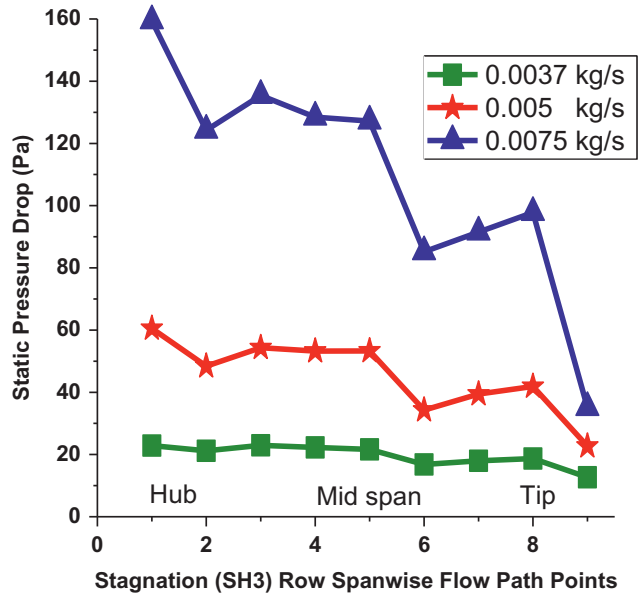


Figure 13: Span wise coolant pressure drop variation at SH3 row holes.

coolant mass flow rates at the FIT plenum. And hence the maximum coolant ΔP_s values are observed as 22.93, 60.52 and 159.40Pa for the consecutive three coolant mass flow rates maintained at the LE circuit of the NGV.

This happens due to the influence of the mainstream velocity at the stagnation row which is ineffective, as the S/C ratio is approximately zero. This suggests that the ejected coolant jet ΔP_s is higher at the hub region holes. On the contrary, the tip region holes exhibit lesser amount of jet ΔP_s . It is mainly because the amount of coolant jet mass flow rate is higher at the hub region holes than the tip region holes, as the coolant jet flow is accelerated in the span-wise direction in the stagnation row.

In the FIT baseline flow rate case, the percentage of coolant ΔP_s variations of this row range from 7.16% (at the ninth hole) to 12.95% (at the third hole). The corresponding minimum percentage values are gradually decreased to 5.56% and 3.36%. The maximum percentage values are increased to 14.83% and 16.20% for the increased FIT flow rates. This is due to the minimum static pressure values that are gradually decreasing from 10.82% to 8.78% at the ninth hole inlet.

Figure 14 depicts the coolant static pressure drop distribution at SH2 row showerhead holes in the span-wise direction. This row is positioned very close to the stagnation row, toward the pressure side of the NGV surface. The SH2 row film cooled holes predicts that the first hole with minimum static pressure difference value 10.43Pa, second hole with maximum static pressure difference value of 22.02Pa at the hub region for the

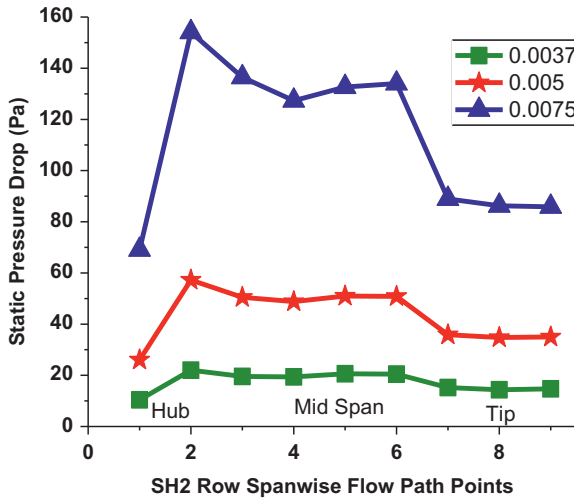


Figure 14: Span wise coolant pressure drop variation at SH2 row holes.

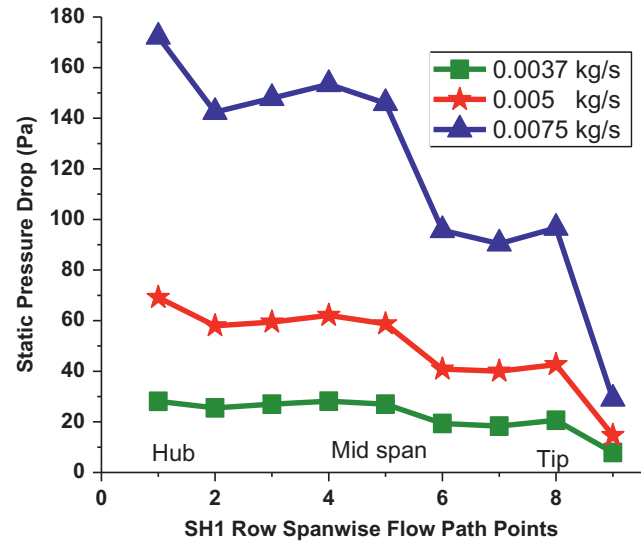


Figure 15: Span wise coolant pressure drop variation at SH1 row holes.

baseline condition. Even after higher coolant mass flow rate was maintained at the FIT channel, the maxima and minima points were obtained at these same holes positions. The only difference was that these pressure difference magnitudes would increase in proportion to the amount of the jet coolant mass rate at the individual hole. The most important thing is that the minimum that ΔP s decreases is by 2.24 Pa in comparison with the stagnation row for the baseline mass flow rate of the FIT plenum. At \dot{m}_c of 0.005 kg/s, the corresponding minimum ΔP s value is slightly improved by 3.36 Pa, whereas this value is largely increased by 33.07 Pa for the 0.0075 kg/s at the FIT plenum. The maximum ΔP s values are obtained as 57.23 Pa and 154.07 Pa for the increased FIT flow rates. This is mainly because the SH2 row is in symmetry with the S/C ratio about SH4 row. Therefore, the behaviour and existence of the minimum and maximum hole positions depicted in Figure 13 are exactly similar to those in Figure 11. The only difference is in the coolant static pressure drop magnitudes. The situation has also been observed by Wright et al. [11] and Chandran et al. [16]. The movement of the streamlines moving toward the pressure surface is less as compared to the suction surface film cooled holes considering from the stagnation row showerhead holes. This, in turn, necessitates the increase in the strength of the counter rotating vortex pair.

Figure 15 illustrates the span-wise variation of the secondary air coolant static pressure drop at the SH1 row showerhead holes. SH1 row is located on the pressure surface of the NGV, which is nearer to the stagnation row. The minimum ΔP s decrease is by 4.76 Pa and 2.52 Pa

and the maximum ΔP s increase is by 5.23 Pa and 6.14 Pa from the SH3 and SH2 rows respectively under the baseline \dot{m}_c condition. However, the minimum ΔP s is observed at the ninth hole, which is placed at the NGV tip region and the same position is continued for the higher \dot{m}_c maintained at the FIT cooling channel. The maximum ΔP s value of 28.16 Pa occurs at the fourth hole (mid-span) for the baseline coolant \dot{m}_c condition. But the next two higher \dot{m}_c in this position are shifted to the first hole of the hub region. In this SH1 row, the minimum ΔP s value is 7.91 Pa at the ninth hole with maximum ΔP s value of 28.16 Pa at the fourth hole for the baseline condition. For the remaining two higher plenum flow rates, the minimum ΔP s values are obtained as 14.62 Pa and 29.11 Pa. Subsequently, the maximum ΔP s values are obtained as 69.19 Pa and 172.16 Pa.

The SH1 row behaviour and the minimum and maximum hole positions resemble those given in Figure 11. Since the SH5 and SH1 rows are symmetry in S/C ratio, considering from stagnation row. The only difference is that the coolant static pressure drop magnitudes are smaller than those of the SH5 row values. This happens because of the effect of the mainstream velocity that gradually decreases, due to the adverse pressure gradient on the PS of the NGV.

Figure 16 illustrates the span-wise area-weighted average coolant static pressure drop distribution at each showerhead row for all the FIT plenum mass flow rates. Figure 15 reveals that the amount of area-weighted average pressure drop values are more at the SH5 and SH4 rows. This is due to the effect of mainstream velocity that is higher at these rows owing to its favorable pressure

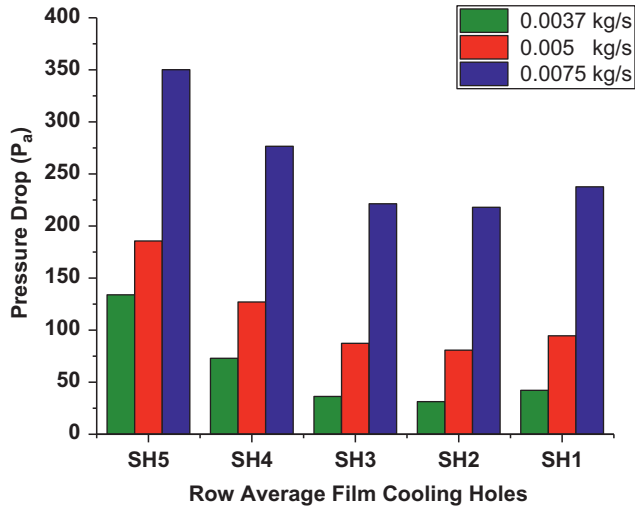


Figure 16: Span wise pressure drop variation on the entire the leading edge of showerhead holes.

gradient on the SS rows. The area-weighted average pressure drop values are lower at the PS rows, namely SH2 and SH1 rows. This happens because of the adverse pressure gradient on the PS of the NGV. Moreover, the SH4 and SH2 rows have smaller area-weighted average pressure drop values. The influence of the mainstream velocity is smaller on these rows, as they are positioned very close to the stagnation (SH3) row. All the showerhead holes on the LE convex shape are positive pressure drop values. This indicates that there is no reversal flow within each film hole, which in turn leads to the Hot Gas Ingestion. This phenomenon should not be allowed for the gas turbine NGV film cooling.

The coolant jet pressure drop variation at each SH row of the film holes on the LE of the NGV surface mainly depends on the amount of the coolant supplied at the FIT plenum, row S/C ratio location and the effect of mainstream on these holes.

Leading edge rows coolant temperature rise distributions

Figure 17 illustrates the static temperature rise variation at SH5 row film cooled holes. This row is located towards the suction surface of the vane. For the baseline flow rate condition, the eighth hole has the minimum ΔT_s value of 0.52936 K, and the first hole has the maximum static ΔT_s value of 0.77316 K.

At increased coolant mass flow rate provided at the FIT channel, the maximum ΔT_s value is to be continued at the first hole, which covers under the hub region. The

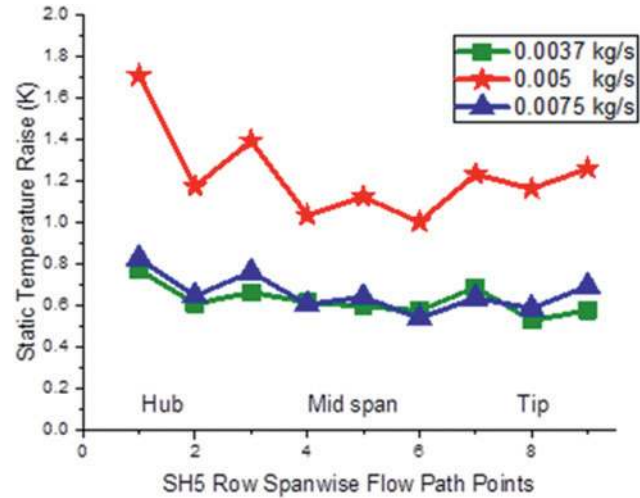


Figure 17: Span wise coolant static temperature rise distribution at SH5 row holes.

minimum ΔT_s values are changed to the sixth hole of this row, which covers at the mid-span region. Moreover, unlike static pressure drop distribution, the coolant static temperature rise in ΔT_s is higher for all the holes of this row, which are attained for the FIT mass flow rate of 0.005 kg/s. This is because when the coolant jet exits from the film hole, it gets detached from the convex surface of the NGV and allows the mainstream flow beneath the jet exit, causing the maximum raise in the convective heat flux values at the interaction surface. The same conclusion is reported by the Panda and Prasad [14].

This is mainly due to the effect of the convective heat flux at the interaction region and also the conductive heat transfer causes within solid NGV surface temperature is higher. For the maximum FIT flow rate of 0.0075 kg/s, the detached jets reattach to the surface of the NGV, so the convective heat flux magnitudes are decreased due to the enhanced lift-off.

The ΔT_s values are slightly improved by a maximum of 0.21% for the flow rate of 0.0075 kg/s in comparison with the 0.0037 kg/s. It is because of the abrupt changes in the vane surface temperature at these two conditions. At m^*_c of 0.005 kg/s, the corresponding minimum ΔT_s value is 1.0039K with an increase in 0.34% at the eighth hole and the maximum ΔT_s value of 1.7071K is achieved at the first hole by an improvement of 1.67%. The S/C ratio is higher for the SH5 row so that the effect of convective heat flux is decreased, which in turn causes a decrease of ΔT_s values for all the plenum flow rates. When the FIT coolant m^*_c is increased to the 0.0075 kg/s, the maximum and the minimum static ΔT_s magnitudes are repeated at the same hole positions as

the previous case, but these magnitudes are arrived as 0.5399K (9.08%) at the and 0.828K (13.93%) respectively.

Figure 18 shows the span-wise variation of the ejected coolant jet static temperature raise for the SH4 row film cooled holes. The coolant static temperature raise (ΔT_s) is the difference between the exit and inlet static temperatures of the film hole. The SH4 row is positioned very close to the stagnation row (S/C ratio = 0.099).

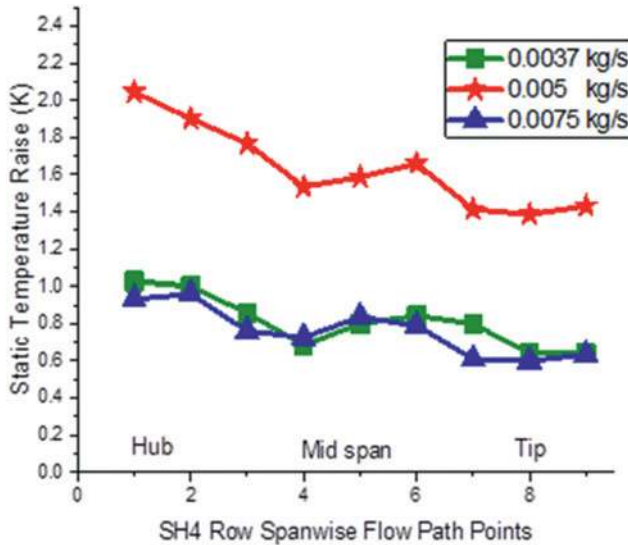


Figure 18: Span wise coolant static temperature rise distribution at SH4 row holes.

The minimum static ΔT_s value of 0.64K occurs at both the eighth and ninth holes with equal ΔT_s magnitudes, whereas the first hole positioned in the hub region has the maximum static ΔT_s value of 1.03K. These magnitudes are observed for the FIT plenum mass flow rate of 0.0037 kg/s. On the other hand the mainstream temperature and velocity are maintained as 303K and 6 m/s respectively.

For the FIT plenum mass flow rate of 0.005 kg/s, the maximum coolant ΔT_s magnitude of 2.04K persists at the same hole position as in the case of 0.0037 kg/s. But, the minimum coolant ΔT_s with a magnitude of 1.39K occurs at the eighth hole. The enhanced ΔT_s magnitudes are basically due to percentage increase of ΔT_s values, which vary from 9.41% to 13.89%.

Similarly, for the highest FIT plenum flow rate of 0.0075 kg/s, the corresponding maximum and minimum static temperature raise magnitudes are obtained as 0.96K and 0.60K respectively. However, the maximum value is arrived at the second film hole of this row,

provided in the hub region. But, the minimum value is noticed similar to the flow rate condition of 0.005 kg/s. This is due to the higher convective heat the loads are subjected to in and around the stagnation region. This makes the higher heat pick-up by the coolant at the SH4 row compared to previous (SH5) row, for all the LE circuit flow rates. Therefore, this necessitates the maximum and minimum coolant ΔT_s magnitudes that are noticed at the hub and tip region of the NGV for a given plenum flow rate and mainstream condition.

The enhanced heat flux values for this row, at the interaction surface, are noticed for the flow rate of 0.005 kg/s. The same trend is depicted as discussed in Figure 17. The only difference is that, the lower convective heat fluxes are observed at the maximum flow rate of 0.0075 kg/s.

Figure 19 shows the coolant static temperature raise variation at the stagnation row (SH3) of the showerhead holes. At the baseline condition, the sixth hole which is located at the mid-span of the NGV is noticed with minimum ΔT_s value of 0.72K. However, the first hole is noticed with maximum coolant ΔT_s value of 0.97K at the hub region. The corresponding percentages vary from 8.98% to 12.04%. As per the detailed explanation made in the earlier rows, the similar convective heat flux effect is observed for the FIT plenum m^*_c of 0.005 kg/s. Except that the maximum and minimum coolant ΔT_s magnitudes with their percentages of variations are predicted as 1.84K (13.39%) and 1.39K (10.11%). These occur at the fifth hole, located at the mid-span and first hole of

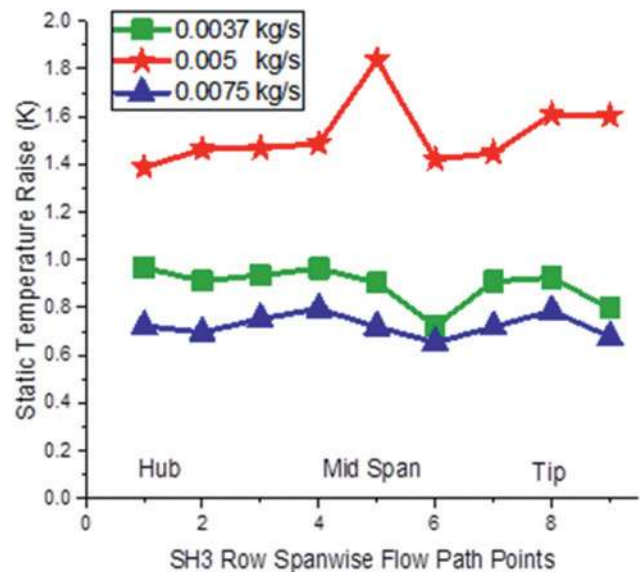


Figure 19: Span wise coolant static temperature rise distribution at SH3 row holes.

this row. Finally, at the FIT plenum \dot{m}'_c of 0.0075 kg/s, the minimum ΔT_s value of 0.65K is noticed at the sixth hole and the maximum ΔT_s value of 0.80K is noticed at the fourth hole. Both the minima and maxima positions are arrived at the mid-span of the row. The ΔT_s percentage values vary from 10.03% to 12.19%. This is due to the strong aerodynamic and thermal interaction surface that exists between the mainstream flow and the ejected coolant jet from the film holes which greatly affects the local convective heat transfer in the stagnation and wall jet regions as well as the average heat transfer over the surface.

Figure 20 illustrates the SH2 row showerhead holes span-wise coolant ΔT_s variation. An analysis of the results indicates that for all the three FIT plenum coolant mass flow rates, the minimum coolant ΔT_s exists at the ninth hole. And the maximum ΔT_s is observed at the first hole of this row. The ninth and first holes are positioned at the tip and hub regions of the NGV surface. The cooling air is impinging on the rear side of the convex shape and enters into the film holes. The ejected film cooled jet, during its passage, picks up heat from the convective heat transfer as well as conductive heat transfer from the film hole solid walls. The amount of heat pick-up due to the impinging action of the jet also depends on the material thermal conductivity chosen for the NGV surface. This happens because of the thicker thermal mixing region at the interaction surface of the SH2 row due to its low free-stream velocities. From the three different FIT plenum coolant flow rates, it is noticed that the

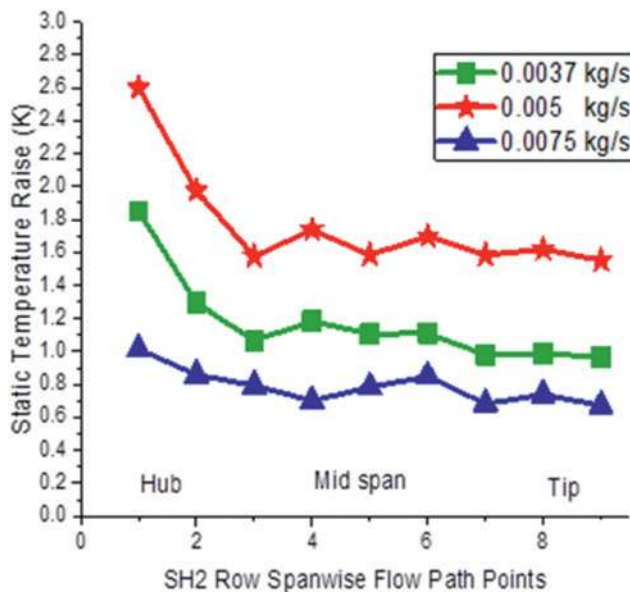


Figure 20: Span wise coolant static temperature rise distribution at SH2 row holes.

inlet and exit coolant static temperatures decrease with an increase in the plenum flow rate. And both the inlet and exit temperatures are higher for the baseline flow rate condition than the higher FIT flow rates.

At the baseline condition, the minimum and maximum ΔT_s values with their percentages are obtained as 0.97K (9.16%) and 1.85K (17.53%) respectively. For the \dot{m}'_c 0.005 kg/s, the corresponding minimum and maximum ΔT_s values are increased by 0.59K and 0.75K respectively. However, the plenum coolant mass flow rate increased to 0.0075 kg/s, then both the minimum and maximum ΔT_s values decreased by 0.88K and 0.84K respectively. Even though, the present row is in symmetry with the S/C ratio about the SH4 row, the existence of the convective heat flux is more on the PS showerhead rows. It is mainly due to higher thermal interaction surface on the pressure surface, which necessitates the higher ΔT_s values for the SH2 row film cooled holes for all the three plenum mass flow rates.

Figure 21 shows the span-wise variation of coolant static temperature raise at the SH1 row showerhead holes. The SH1 row is positioned toward the pressure surface of the NGV, which is far from the stagnation row.

For the baseline flow rate condition, the minimum ΔT_s value of 0.69K is noticed at the ninth hole, which covers the tip region. The maximum ΔT_s value of 1.0K is noticed at the second hole, which covers the hub region. For the subsequent higher plenum coolant mass flow rates, the maximum and minimum ΔT_s locations of the film holes are observed at the fourth and first holes of

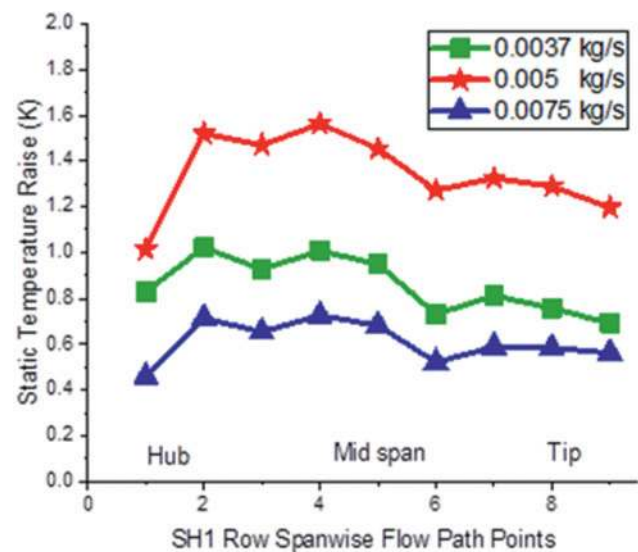


Figure 21: Span wise coolant static temperature rise distribution at SH1 row holes.

this row. For the FIT plenum, m'_c is increased to 0.005 kg/s, both the minimum and maximum ΔT s values are obtained as 1.01K and 1.56K. Similarly, for the plenum maximum flow rate of 0.0075 kg/s, both the minimum and maximum ΔT s values are noticed as 0.46K and 0.73K. Similar trends are observed on par with SH5 row as both of them are in symmetry about S/C ratio. However, there exists a difference in the static temperature raise values and their locations. Moreover, the three FIT plenum m'_c reveal that the SH1 row showerhead holes have decreased coolant ΔT s values as compared to SH2 row film cooled holes. This happens due to the effect of the convective heat load on the interaction surface of the SH1 row that is lowered at the downstream of the stagnation point.

Figures 22 shows the span-wise coolant static temperature raise variation at each showerhead row film holes for the three different plenum flow rates. Film cooled jet exit temperatures approach the FIT plenum coolant inlet temperature, which tends to occur at a higher momentum. This is because the coolant flow has been less influenced by the mainstream flow. This necessitates a fully developed FIT plenum coolant flow followed by the heat transfer. This is because the stagnation temperature is affected by the film hole jet exit momentum or velocity. For an NGV, both the stagnation temperature and static temperatures are the same.

The film holes at each showerhead row experience that the coolant jets have been noticed with non-uniform static temperature distribution both at the inlet and exit of the hole. It is due to the influence of convective heat flux from hole to hole at each SH row. For the baseline

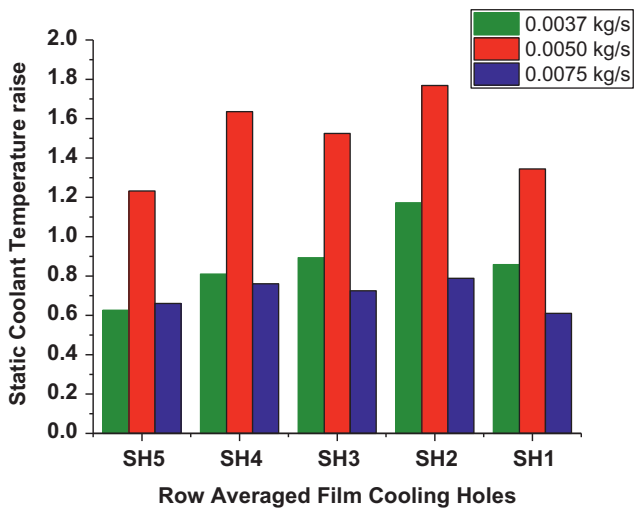


Figure 22: Comparison of area weighted average static temperature raise for all the showerhead rows of the film cooled hole positions.

flow rate condition, the film cooled jet exit has low cross flow momentum, which allows the increase of convective heat transfer on the interaction surface. Conversely, the NGV conductive heat transfer increases. In the case of the maximum FIT plenum flow rate of 0.0075 kg/s, the influence of the convective heat transfer to the effused coolant jet at each row of the film holes decreases. Simultaneously, the conduction of the blade wall increases.

For the FIT plenum coolant mass flow rate of 0.005 kg/s, the enhanced ΔT s magnitudes are basically due to the percentage increase of both the inlet and exit static temperature magnitudes in the span-wise direction. Similar observations are noticed by Singh etAl. [20] with the increase in the ratio of spacing between two jets to nozzle diameter (s/d), the average Nusselt number over the cylinder surface increased. The optimal value of jet spacing is obtained at $s/d=20$ for maximum average Nusselt number.

Conclusions

Numerical study on a three-dimensional conjugate heat transfer of a combined impingement and film cooled gas turbine nozzle guide vane is investigated. Different combinations of mainstream Reynolds number and coolant mass flow rates, supplied at the FIT plenum, are the input parameters in the present study. The following conclusions are drawn from the numerical study:

1. All the three different FIT plenum coolant mass flow rates, more coolant flows into the tip region of the film holes whereas smaller quantity of coolant is available near the hub region of the film holes in each showerhead row film hole. This is because of strong counter-rotating vortices formation that is associated with the jetting effect which weakens at the higher FIT plenum flow rates and the ejected coolant jets in the tip region of the holes have sufficient momentum.
2. The total coolant mass flow ratio is higher at the SH5 and SH4 rows, which are positioned toward the SS region, than the SH1 and SH2 rows, which are positioned toward the PS of the NGV. This is due to the favorable pressure gradient for the SH4 and SH5 rows. Furthermore, the showerhead film holes have 65% to 67% of the total supplied FIT coolant mass flow rate that is achieved for all the three plenum flow rates. It mainly depends on the amount of the coolant supplied at the FIT plenum, span-wise inclination of the holes and each SH row

S/C ratio on the convex shape of the LE circuit of the NGV.

3. The coolant pressure drop trends are on par with the mass flow rate trends, because for the incompressible flow, the mass flow rate directly relates to the pressure drop. This ensures that the SH5 and SH4 rows exist at higher pressure drop magnitudes than the SH2 and SH1 rows. In addition to that, the SH5 and SH1 rows are in symmetry in the S/C ratio, which results in the same trends. The minimum and maximum hole positions occur at the ninth and first holes of the row. But, these ΔP s magnitudes increase with an increase of the mainstream velocity at this row. This causes a decrease in the solid surface temperature of the film holes. Similarly, SH4 and SH2 rows attain symmetry in S/C. Therefore, these rows show the same trends; the minimum and maximum hole positions occur at the first and second holes of the row. As these rows are positioned very close to the stagnation (SH3) row, the effect of mainstream velocity is small.
4. Each SH row film cooled holes on the convex shape of the LE circuit of the NGV shows positive pressure drop values. This reveals that there is no reversal flow within each film hole, which will be subjected to the hot gas ingestion effect. The effect of hot gas ingestion is not acceptable for the safety and durability of the NGV.
5. The calculated minimum static pressure drop across the specified rows of the film cooled holes is primarily due to insufficient cross flow momentum of the ejected coolant jet. And the occurrence of the maximum static pressure drop at a particular row of the film cooled holes is due to the attained sufficient cross flow momentum of the effused coolant jet. These coolant static pressure drop magnitudes increase in proportion to the amount of the higher coolant mass flow rates maintained at the FIT plenum.
6. The S/C ratios are higher for the SH1 and SH5 rows from the SH3 row, the locations at which the effect of LE curvature is higher. This will be subjected to lower convective heat flux on the interaction surface region. However, SH2 and SH4 rows film cooled holes are noticed with the higher coolant ΔT s magnitudes. The heat pick-up by the coolant on the interaction surface regions of the rows is higher as these S/C ratios are very close to the stagnation row.
7. The maximum coolant temperature raise magnitudes in the span-wise direction at each SH row film holes occur for an FIT plenum flow rate of

0.005 kg/s, considering the constant mainstream temperature and velocity. This is mainly due to both the convective heat transfer to the ejected film cooling jet and the conductive heat transfer through the NGV wall.

8. The CFD analysis for the coolant flow path behavior of a combined impingement and film cooled NGV provides the nonlinear variation of both the coolant static pressure drop and coolant static temperature raise at each showerhead (SH) row of the film cooled holes for a given FIT coolant mass flow rate, mainstream velocity, mainstream turbulent intensity and mainstream temperature. This suggests that considering these parameters as design variables needs to optimize the secondary coolant flow for the conflicting objectives of the minimization of the coolant static pressure drop and maximization of the coolant static temperature raise to ensure safety and durability of the NGV surface.
9. The computational time taken for each simulation is approximately four to five days on a DELL system, core-i5, 96GB RAM work station, but it is extremely time intensive and its use to analyze the optimization of multiple configurations are cumbersome. Therefore, a fast and efficient method of thermo-fluid one-dimensional network modeling technique is recommended for future investigations. The reason is that the 1D computations are achieved within one minute time duration for the same boundary conditions. But the development of 1D model for this typical configuration will be extremely difficult, equivalent to the 3D CFD model. However, the modular nature of the network representation provides the various parametric studies, for the efficient and rapid method for the multi-objective optimization of the secondary coolant flow analysis of a combined impingement and film cooled gas turbine NGV.

Nomenclature

\dot{m}	- Mass flow rate (kg/s)
P	-Pressure (Pa)
ΔP	-Pressure Drop (Pa)
T	-Temperature (K)
ΔT	- Coolant Temperature Raise (K)
S	- Streamwise distance from the stagnation point to the specified row position
C	-True chord length of the vane

Subscript

i	inlet
o	outlet

t	Total
s	Static
j	Film cooled jet location
c	Summation of film cooled row total values

Abbreviations

CFD	-Computational Fluid Dynamics
NGV	-Nozzle Guide Vane
FIT	-Front impingement tube
PS	Pressure Surface
SS	Suction Surface
LE	Leading Edge
SH	Showerhead

IL Impingement rows facing the leading edge region.

References

- Goldstein RJ, Timmers JF. Visualization of heat transfer from arrays of impinging jets. *Int J Heat Mass Transf* 1982;25:1377–1382.
- Honami S, Shizawa T, Uchiyama A. Behavior of the laterally injected jet in film cooling: Measurements of surface temperature and velocity/temperature field within the jet. *J Turbomachinery* 1994;116:106–112.
- Huang Y, Ekkad SV, Han JC. Detailed Heat Transfer Distributions Under an Array of Orthogonal Impinging Jets. *AIAA J Thermophysics Heat Transfer* 1998;12:73–79.
- Ekkad SV, Han JC. Heat Transfer Distributions on a Cylinder with Simulated Thermal Barrier Coating Spallation. *J Thermophysics Heat Transfer* 1999;13:76–81.
- Ekkad SV, Huang Y, Han JC. Impingement Heat Transfer on a Target Plate with Film Cooling Holes. *AIAA J Thermophysics Heat Transfer* 1999;13:522–528.
- Heidmann JD, Rigby DL, Ameri AA. A Three-dimensional coupled internal/external simulation of a film-cooled turbine vane. *J Turbomachinery* 2000;122:348–359.
- Gritsch M, Schulz A, Wittig S. Effect of internal coolant cross-flow on the effectiveness of shaped film-cooling holes. *J Turbomachinery* 2003;125:547–554.
- Gao L, Ekkad SV, Bunker RS. Impingement Heat Transfer Part I: Linearly Stretched Arrays of Holes. *AIAA J Thermophysics Heat Transfer* 2005;19:57–65.
- Katti V, Prabhu SV. Influence of spanwise pitch on local heat transfer distribution for in-line arrays of circular jets with spent air flow in two opposite directions. *Exp Thermal Fluid Sci* 2008;33:84–95.
- Oh SH, Lee DH, Kim KM, Kim MY “Enhanced Cooling Effectiveness in Full-Coverage Film Cooling System with Impingement Jets”, *Proceedings of ASME Turbo Expo, GT2008–50784*, 2008.
- Wright LM, McClain ST, Clemenson MD. Effect of freestream turbulence intensity on film cooling jet structure and surface effectiveness using PIV and PSP. *J Turbomachinery* 2011;133:041023–1–041023-12.
- Jessen W, Konopka M, Schroder W. Particle-image velocimetry measurements of film cooling in an adverse pressure gradient flow. *J Turbomachinery* 2012;134:0210251–02102513.
- El-Gabry LA, Thurman DR, Poinsatte PE, Heidmann JD. Detailed velocity and turbulence measurements in an inclined large-scale film cooling array. *J Turbomachinery* 2013;135:0610131–06101311.
- Panda RK, Prasad BVSSS. Conjugate Heat Transfer from an Impingement and Film-Cooled Flat Plate. *AIAA J Thermophysics Heat Transfer* 2014;28(4):647–666.
- Pujari AK, Prasad BVSSS, Sitaram N “Heat Transfer Studies on the Interior surfaces of Cooled Nozzle Guide Vane in a Linear Cascade”, *Proceedings of ASME Turbo Expo, GT2015-43972*, June 15-19, 2015, Montreal, Canada.
- Chandran D, Prasad B. Conjugate heat transfer study of combined impingement and showerhead film cooling near NGV leading edge. *Int J Rotating Machinery* 2015; 2015:1–13.
- Singh D, Premachandran B, Kohli S. Circular air jet impingement cooling of a circular cylinder with flow confinement. *Int J Heat Mass Transf* 2015;91: 969–989.
- Singh D, Premachandran B, Kohli S. Effect of nozzle shape on jet impingement heat transfer from a circular cylinder. *Int J Thermal Sci* 2015;96:45–69.
- Pujari AK, Prasad BVSSS, Sitaram N. Effect of blowing ratio on the internal heat transfer of a cooled nozzle guide vane in a linear cascade. *ASME J Thermal Sci Eng Appl* 2016;8:0410041–04100415.
- Singh D, Premachandran B, Kohli S. Double circular air jet impingement cooling of a heated circular cylinder. *Int J Heat Mass Transf* 2017;109:619–646.
- Kukutla PR, Prasad BVSSS. Secondary flow visualization on stagnation row of a combined impingement and film cooled high pressure gas turbine nozzle guide vane using PIV technique. *J Visualization* 2017; (Paper Accepted). DOI:10.1007/s12650-017-0434-6